Indentation size and loading strain rate dependent creep deformation of nanocrystalline Mo

J. Zhao[a], P. Huang[b,*], K.W. Xu[b], F. Wang[a,*], T.J. Lu[a,c]

[a] State Key Laboratory for Strength and Vibration of Mechanical Structures, School of Aerospace, Xi'an Jiaotong University, Xi'an 710049, China
[b] State-Key Laboratory for Mechanical Behavior of Material, Xi'an Jiaotong University, Xi'an 710049, China
[c] MOE Key Laboratory for Multifunctional Materials and Structures, Xi'an Jiaotong University, Xi'an 710049, China

ARTICLE INFO

ABSTRACT

The creep behavior of nanocrystalline body-centered cubic Mo thin films was evaluated using nanoindentation testing. The creep rate and the corresponding strain rate sensitivity (m) were found to be strongly dependent upon indentation size and loading strain rate (LSR). Other than the mechanism of diffusion along indenter tip-sample interface previously proposed for face-centered cubic metals and metallic glasses, alternative mechanisms involving surface effect enhanced screw dislocation activities, inverse indentation size effect of hardness and LSR dependent microstructural and stress states, were proposed to interpret the observed dependence of penetration depth and LSR of m.

1. Introduction

Body-centered cubic (bcc) materials, especially refractory metals (e.g., Mo) widely applied in nuclear and defense industry, have been extensively studied in the past decades [1–7]. In particular, refractory metals with nanoscale grain sizes have attracted enormous attention [8], due to their high melting temperature (generally higher than 1800 °C) and excellent mechanical properties, such as enhanced strength, hardness and wear resistance. Creep is a time-dependent plastic deformation usually occurring at elevated temperature under applied stress [9–11]. For nanocrystalline (NC) metals, the high volume fraction of grain boundaries (GBs) could result in enhanced creep deformation even at room temperature, thus strictly limiting their applications as structural materials. Great efforts were thence devoted to evaluating and interpreting the creep deformation behavior of NC metals [12–16]. Compared with the extensive work related to the other mechanical properties of bcc metals [1–4,6], most of existing studies on creep were based on face-centered cubic (fcc) metals, with only few focusing on bcc metals [17,18], especially for NC bcc metals.

Different from fcc metals, screw dislocation related deformation mechanisms dominated the plastic deformation of bcc metals [19,20]. Moreover, the density of screw dislocations was found to be grain size dependent as no pure screw dislocation could exist when the grain size was below a critical length scale about 100 nm [21]. More importantly, numerous studies indicated that NC bcc metals exhibit a much smaller strain rate sensitivity index m than their coarse grained counterparts

[19,20,22,23]. Even though improved understanding has been achieved based on the aforementioned studies, the mechanisms controlling the creep behavior of NC bcc metals and how the microstructural and deformation length scales affect the time-dependent plasticity are still unclear and even subjected to intensive debate.

To evaluate the creep behavior, nanoindentation testing was widely applied as an effective experimental technique for probing creep parameters, such as the stress exponent [14], the activation volume [24,25] and the strain rate sensitivity [26,27], which have been found to exhibit a strong dependence on penetration indentation depth [28,29]. Therefore, in the present study, the creep behavior of magnetron sputtering fabricated NC Mo thin films and its dependence on penetration indentation depth and loading strain rate (LSR) were characterized using nanoindentation testing. The controlling creep mechanism and related size effects were proposed and discussed.

2. Experiments

2.1. Sample preparation

NC bcc Mo films with a fixed thickness of 1350 nm were deposited via *d.c.* magnetron sputtering on single silicon wafer using high purity target Mo (purity of 99.999%). The direct current sputtering power of Mo target was 100 W, and the deposited rate was about 7 nm/min. The microstructures of Mo were investigated by the high resolution transmission electron microscopy (HRTEM, JEOL 2100F, Tokyo, Japan)
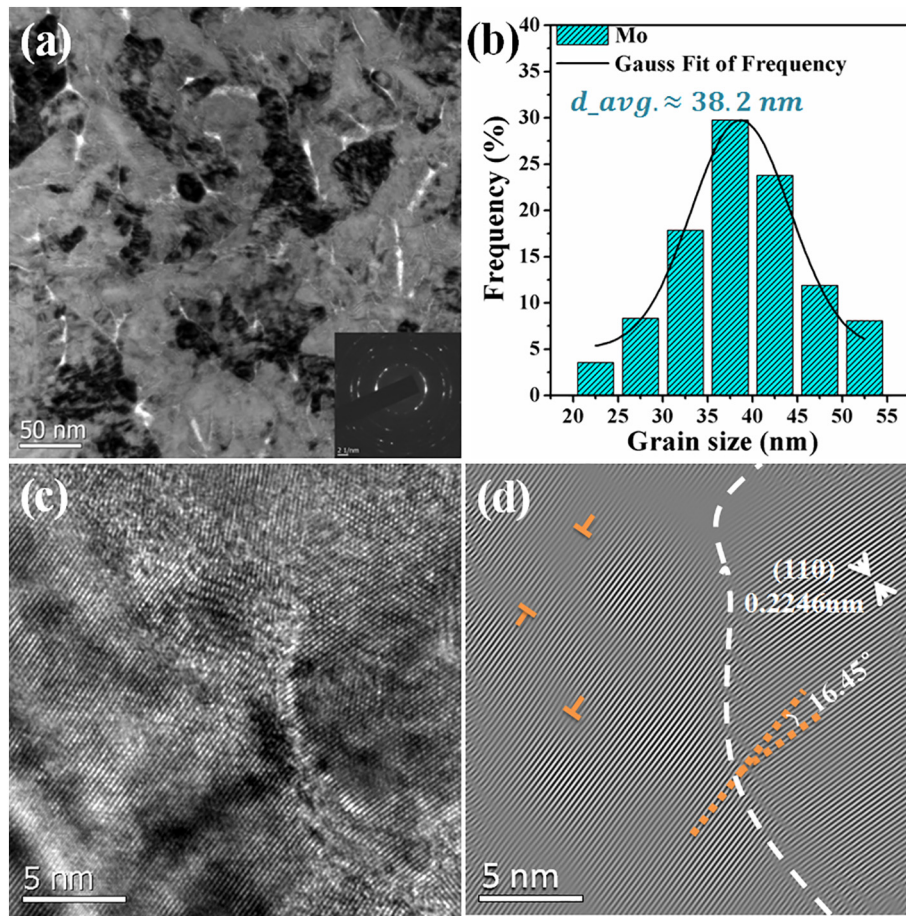
Fig. 1. (a) TEM bright-field image and (b) grain size distribution of bcc-Mo film. (c) HRTEM image of NC Mo film and (d) Inverse Fourier-filtered image of (c).

under accelerating voltage of 200 kV. And the TEM foils were prepared and fabricated by ion beam milling technique via Gatan Precision Ion Polishing System 691.

2.2. Nanoindentation creep testing

Nanoindentation creep tests with different LSR ranging from $0.005\,s^{-1}$ to $0.2\,s^{-1}$ were carried out using MTS Nanoindenter XP® system (MTS, Inc) under Continuous Stiffness Measurement (CSM) mode. The dwell time was set to be 100 s at each LSR in order to evaluate the creep behavior of the NC Mo. The radius of the Berkovich diamond indenter was ~50 nm. In addition, the creep tests were conducted by depth control mode with the penetration depth varying within the range from 15 nm to 200 nm (< 1/7 thickness of the Mo film to avoid substrate effects [30]). Eventually, each test was performed 12 times, and at least 8 effective data were involved in eventual analysis.

3. Results

Fig. 1(a) shows the plan-view bright field micrograph of the Mo film, with the right bottom corner displaying the corresponding electron diffraction patterns. The average grain size was statistically calculated by HRTEM analysis and the grain size distribution fitted normal distribution was presented in Fig. 1(b), which indicated the average grain size is about 38.2 nm. Moreover, a large amount of dislocations (including both edge and mixed dislocations [31]) could be observed at the area closer to grain boundaries, where the density of dislocations is estimated to be about $10^{16}\,m^{-2}$ [31], and the width of grain boundary is ~2 nm as shown in Fig. 1(c–d).

Fig. 2(a) displayed representative load-displacement (P-h) curves

upon nanoindentation testing for various penetration depths at a fixed LSR of $0.1\,s^{-1}$. The platform in each curve represented the load holding regime where the applied stress was constant, as shown in Fig. 2(a). Meanwhile the constant applied stress at holding regime enhanced with increasing set indentation depth and LSR. Also, the curves for creep displacement versus holding time were presented in Fig. 2(b), providing deeper penetration depth results in larger creep displacement, with the end of the curves generally assumed to be the steady-state creep period. Eventually, the LSR dependent creep curves were shown in Fig. 2(c), which indicated that faster LSR leads to larger creep displacement. Similar trends were reported in NC fcc-Cu [31], tetragonal-Ta [32], and even metallic glasses [33].

The creep rate $\dot{\varepsilon}_{creep}$ of a crystalline metal could be empirically described as [34]:

$$\dot{\varepsilon}_{creep} = \frac{AD_0Gb}{kT}\left(\frac{b}{d}\right)^p\left(\frac{\sigma}{\mu}\right)^n\exp\left(-\frac{\Delta Q}{kT}\right)$$

(1)

where σ is the applied stress, A is a coefficient related to temperature and microstructure, D_O is the diffusion coefficient, G is the shear modulus, ΔQ is the activation energy for thermal-activated process, n is the stress exponent, p is the grain size exponent, k is the Boltzmann constant, T is the temperature, b is the Burgers vector and d is the grain size. For uniaxial tensile testing, metals can exhibit significant creep deformation only at temperatures higher than about half the melting temperature T_m. For nanoindentation creep testing, in contrast, the giga-pascal stress generated under the indenter could induce significant creep deformation even at room temperature. Even though the highly non-homogeneous stress state and continuously expanding deformation volume under the indenter lead to a deformation behavior quite different from that under uniaxial tension, it has been well established that
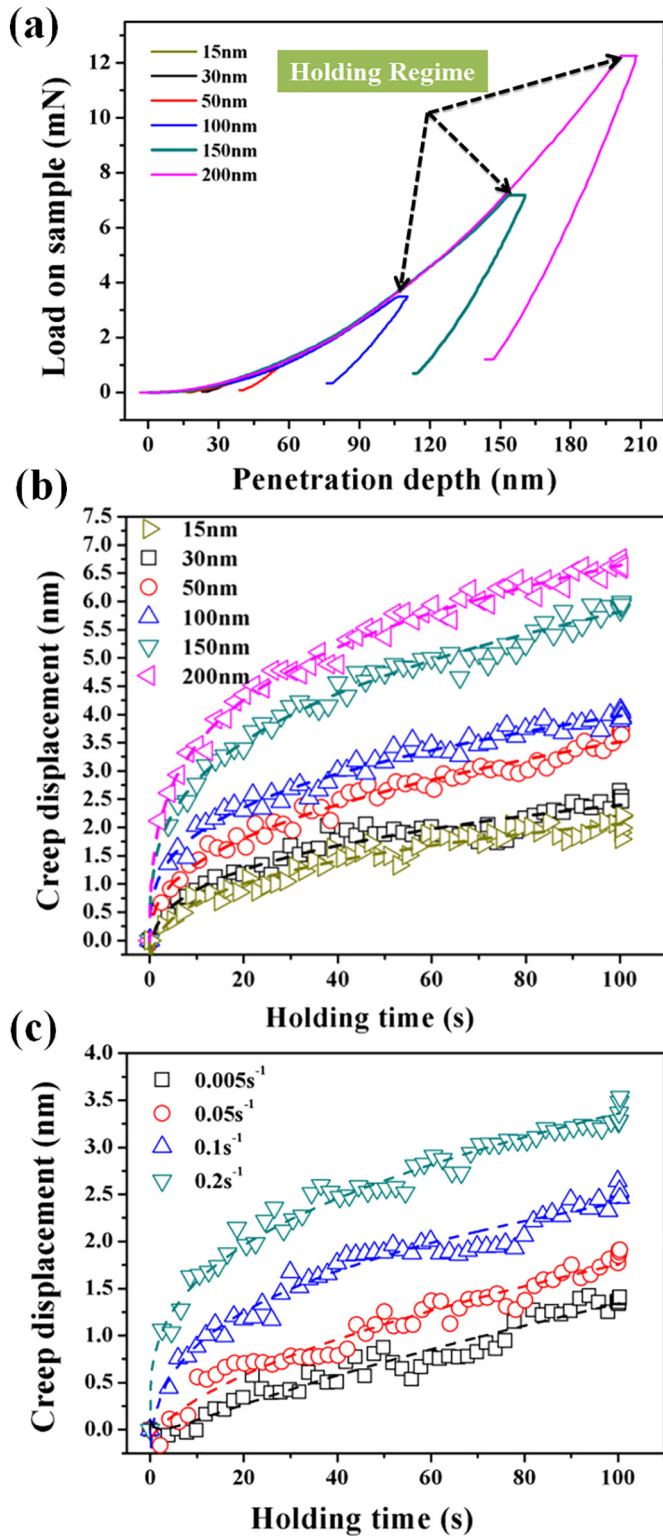
Fig. 3. Creep strain rate ($\dot{\varepsilon}_{creep}$) plotted as a function of penetration depth (h) at selected LSRs (0.005–0.2 s^{-1}).

$$\dot{\varepsilon}_{creep} = \frac{1}{h}\frac{dh}{dt} \tag{2}$$

where h is the instantaneous indentation depth, t is the time, and dh/dt represents the displacement upon indentation testing. Then, the curve of h versus t could be fitted using an empirical equation, as [28]:

$$h = h_i + a(t - t_i)^{0.5} + b(t - t_i)^{0.25} + c(t - t_i)^{0.125} \tag{3}$$

where a, b and c are the fitting constants, and h_i and t_i are the penetration depth and initial time at the onset of creep, respectively. The dash dot lines in Fig. 2(b–c) represented the corresponding fitting curves for creep displacement versus time. Based on Eqs. (2) and (3), the creep rates were derived as shown in Fig. 3. Apparently, the creep rate increased with shallower penetration depth and larger LSR. In addition, the stress could be given by:

$$\sigma = \frac{P}{24.56h^2} \tag{4}$$

where P is the instantaneous applied indentation load right before creep, and h is the instantaneous indentation depth during creep process. Then, the strain rate sensitivity index m could be estimated from typical double logarithmic curve of stress σ versus creep rate, as [27,29]:

$$m = \partial \log \sigma / \partial \log \dot{\varepsilon}_{creep} \tag{5}$$

The values of m derived for each test were presented in Fig. 4, which were significantly dependent upon indentation size effect (ISE) and LSR: m increased with decreasing penetration depth and slower LSR.
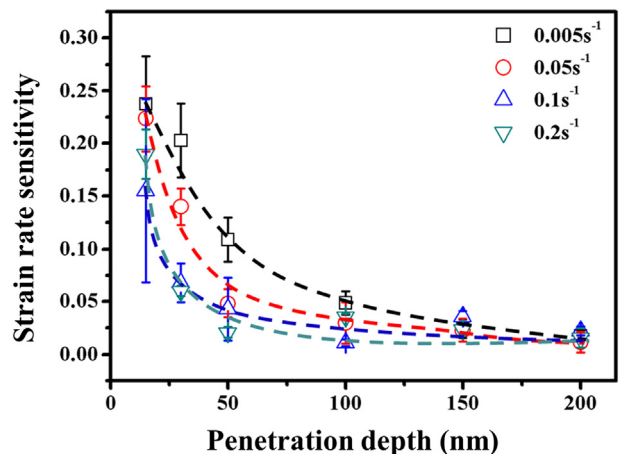
Fig. 4. Strain rate sensitivity (m) plotted as a function of penetration depth (h) at selected LSRs (0.005–0.2 s^{-1}).

Fig. 2. (a) Representative load versus penetration depth curves for selected penetration depths ranging from 15 nm to 200 nm, at LSR of 0.1 s^{-1}, (b) typical creep displacement versus holding time curves at selected penetration depths at LSR of 0.1 s^{-1} and (c) creep curves at creep depth of 50 nm.

the results derived from indentation creep testing is comparable to those derived from tensile testing.

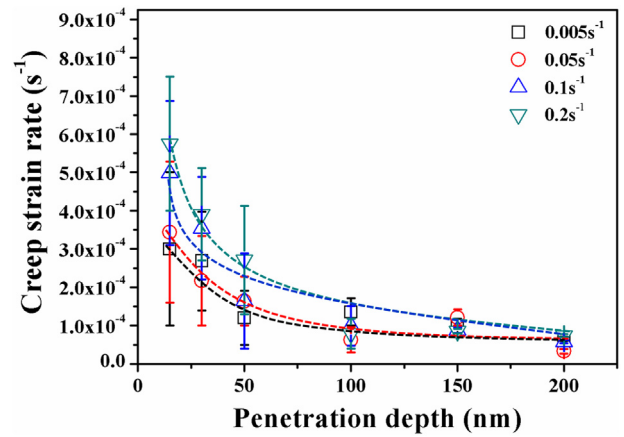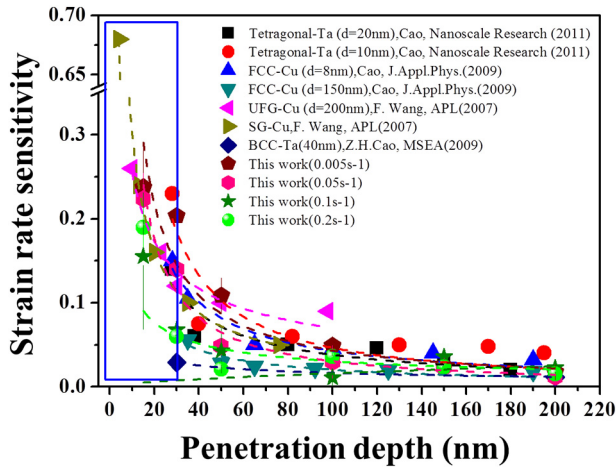For indentation creep, the strain rate applied via Berkovich indenter could be expressed as [35]:

Fig. 5. Strain rate sensitivity (*m*) plotted as a function of penetration depth (*h*) for selected metals, with the references [29,36–38] and the first author corresponding to each data point given.

4. Discussion

The ISE of *m* as observed in Fig. 4 is not new as similar trends were reported in metallic materials with a variety of lattice structures and even in metallic glasses [29,36–38] as shown in Fig. 5. Numerous deformation mechanisms such as diffusion along indenter-sample interface, GBS, Coble creep and dislocation power-law creep had been proposed to interpret the depth dependent creep behavior. As the atomic structures of the aforementioned materials were quite different, the dominating mechanism corresponding to the ISE might be distinct from each other. Therefore, the ISE of *m* for bcc metals with unique atomic structures such as non-plannar core structure of screw dislocation [19] may indeed be dominated via mechanisms different from those of fcc or tetragonal metals [39], as discussed in the following.

Despite the quite different plastic deformation mechanisms among metallic glasses, fcc latticed and bcc latticed metals, similar penetration depth dependent *m* was observed in these materials as shown in Fig. 4. For fcc metals and metallic glasses, diffusion along indenter-sample interface was proposed to dominate their ISE of *m*, and the ISE was effectively reduced as the indenter penetrated deeper where the free surface was getting further away. Other than interfacial diffusion, however, alternative mechanisms might operate in bcc metals as discussed below.

4.1. Diffusion creep mechanisms

First of all, creep deformation occurred within nanoscale grain size of the present Mo thin film, and the ISE of *m* existed at each LSR as shown in Fig. 5. Specifically, *m* increased from ~0.025 to ~0.24 with decreasing penetration depth at LSR of $0.05\,s^{-1}$. In general, the (*n*, *P*, ΔQ) in Eq. (1) was used to distinguish the different dominated creep mechanism [40], such as, $(1, 3, \Delta Q_{GB})$, $(1, 2, \Delta Q_L)$, $(2, 3, \Delta Q_{GB})$ and $(> 4, 0, \Delta Q_L)$ were corresponding to the Coble (GB diffusion), Nabarro-Herring (Lattice diffusion), GBS and dislocation power-law creep, respectively. Apparently, the diffusion creep mechanism (the former two) could be characterized by $n = 1$. Whatever, the value of *m* is inversely proportional to the stress exponent *n* ($m = 1/n$), which suggested the diffusion mechanism and the dislocation power-law creep could also be described by $m = 1$ and $m < 0.25$. Therefore, this observation indicated transition of creep deformation mechanism, as *m* increasing from 0 to approaching 1 had been taken as evidence for transition from dislocation to diffusion creep mechanism, such as Coble creep [41], GBS [42] and Nabarro-Herring diffusion creep [43].

For the present refractory Mo with large fraction of GB, its high

melting temperature (~2883 K) suggested that lattice diffusion governed by Nabarro-Herring mechanism could hardly operate at room temperature. Also, as the activation energy of Nabarro-Herring diffusion is much higher than that of Coble creep and GBS, the latter are much easier to operate in NC metals. Nabarro-Herring diffusion was therefore ruled out as the dominating mechanism.

Alternatively, the attribution of GB related creep mechanisms (i.e., GBS and Coble creep) for creep rate could be calculated as [27]:

$$\dot{\varepsilon}_{GBS} = 2 \times 10^5 D_b \frac{\mu b}{kT}\left(\frac{b}{d}\right)^3\left(\frac{\sigma_s}{\mu}\right)^2 \tag{6}$$

$$\dot{\varepsilon}_{Coble} = A\frac{\sigma_s \Omega \delta D_b}{\pi d^3 kT} \tag{7}$$

where *k* is the Boltzmann constant, *b* is the Burger vector, μ is the shear modulus, σ_s is the stress, Ω is the atomic volume, and δ is the effective diffusive thickness of GB. The diffusion coefficient (D_b) is related to temperature by an Arrhenius-type equation, as [39]:

$$D_b = D_0 \exp\left(-\frac{Q}{RT}\right) \tag{8}$$

where *Q* is the activation energy of diffusion. The vacancy and atoms are not easy to diffuse while the *Q* is large.

For Mo, the relevant parameters as aforementioned were listed as: $b = 2.73 \times 10^{-10}\,m$, $\mu = 1.34 \times 10^5\,MN/m^2$, $Q = 263\,KJ/mol$, $D_0 = 5.5 \times 10^{-14}\,m^3/s$, $\Omega = 1.53 \times 10^{-29}\,m^3$, $\delta = 2b$, $R = 8.314\,J/(mole\cdot K)$ [39]; σ_s was derived from the calculated instantaneous stress upon nanoindentation testing. Then, the calculated creep rates corresponding to GBS and Coble creep of Mo were deduced as shown in Fig. 6. The creep rates calculated with Eqs. (6) and (7) were several magnitudes lower than those derived from nanoindentation testing as shown in Fig. 3. Hence, GBS and Coble creep could also be ruled out as the dominating deformation mechanism. Indeed, the values of *m* shown in Fig. 5 were all much smaller than that of Coble creep ($m = 1$) and GBS ($m = 0.5$), confirming the argument based on creep rate analysis shown in Fig. 6.

4.2. Dislocation creep mechanisms

It was well documented that plastic deformation of bcc metals was generally dominated by screw dislocation kink-pair nucleation, and the core structure of screw dislocations was non-plannar, spreading into various lattice planes. Then, different from fcc metals that exhibited higher *m* at smaller grain sizes, bcc metals generally showed opposite trend as higher *m* appeared at larger grain size [19]. The higher *m* in coarse-grained bcc metals was believed to be closely related to the
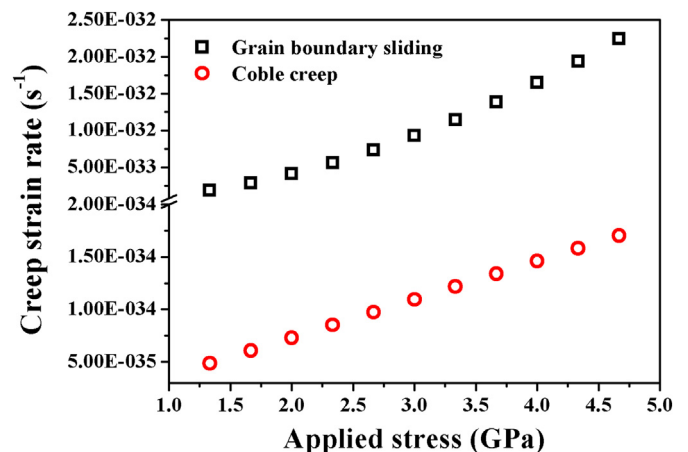

Fig. 6. Creep strain rate plotted as a function of instantaneous applied stress calculated based on GBS and Coble creep mechanism.

movement of screw dislocations, and *m* would be effectively reduced as screw dislocation density monotonically decreased with decreasing grain size [21].

For NC Mo, specifically, Cheng et al. [21] indicated that screw dislocation density monotonically decreased as grain size *d* was decreased, and nearly vanished when $d < 100$ nm, for only pure edge and mixed dislocations remained when 30 nm $< d < 100$ nm. As the grain size of the present NC Mo was estimated to be 38.2 nm, it was reasonable to deduce that the dislocations of Mo thin films were pure edge and mixed dislocations. Therefore, the value of *m* derived at deeper penetration depths, which represented the intrinsic rate dependent strength of NC Mo, should be small. Under such circumstances, the attribution derived from dislocation mechanism to *m* was discussed immediately below.

For the present NC Mo, the dislocation structures consisted mainly of pure edge dislocation and mixed dislocation (containing screw and edge components) [21,44]. As the mobility of edge and screw components/dislocations were quite different in bcc metals, the strain rate sensitivity could be described as [19]:

$$\frac{1}{m} = \frac{\partial \ln \dot{\gamma}}{\partial \ln \tau} \qquad (9)$$

where τ is the shear stress and $\dot{\gamma}$ is the strain rate, which could be obtained using the Orowan equation, as [44,45]:

$$\dot{\gamma} = \rho_s b_s v_s + \rho_e b_e v_e \qquad (10)$$

Here, ρ is the dislocation density, *b* is the Burgers vector, and *v* is the mobility speed. The subscripts *s* and *e* represented edge and screw components/dislocations, respectively.

Similar to the mechanism that kink-pair nucleation of screw dislocation led to higher *m* in coarse-grained bcc metals, the screw-component in a mixed dislocation might also cause increased *m*. The increment of *m* could be enhanced at shallow penetration depths due to a special surface effect working on screw dislocation [46]. Specifically, a compression test on Mo pillar indicated that screw dislocation mobility could be enhanced in the region where free surface was nearby, and that the surface affected zone could be larger than 1 µm [46]. In the present study, all the penetration indentation depths were within the surface affected zone. Therefore, the value of *m* was mainly attributed by the mobility of screw components, which would increase as the penetration depth (especially $h < 100$ nm) was reduced (where the surface effect was enhanced). Under such conditions, the value of *m* was mainly dominated by the slip of the screw-components in a mixed dislocation, as:

$$\frac{1}{m} = \frac{\partial \ln \dot{\gamma}}{\partial \ln \tau} \approx \frac{\partial \ln \rho_s b_s v_s}{\partial \ln \tau} \qquad (11)$$

4.3. The effects of strength on m

Other than the surface effect, the ISE of *m* might also be attributed to the strength/hardness of NC Mo. In our previous study [44], inverse ISE concerning the hardness of the present NC Mo was identified, for its hardness decreased with decreasing penetration indentation depth. Built upon the analysis of Wei [19], the strain rate sensitivity could be described as:

$$m = 3\sqrt{3} \frac{kT}{H \times V^*} \qquad (12)$$

where *H* is the indentation hardness, and V^* is the apparent activation volume representing the area swept out by a gliding dislocation at activation event. In general, the motion of screw components/dislocations is facilitated by kink-pair nucleation mechanism. Therefore, V^* could be expressed as [20];

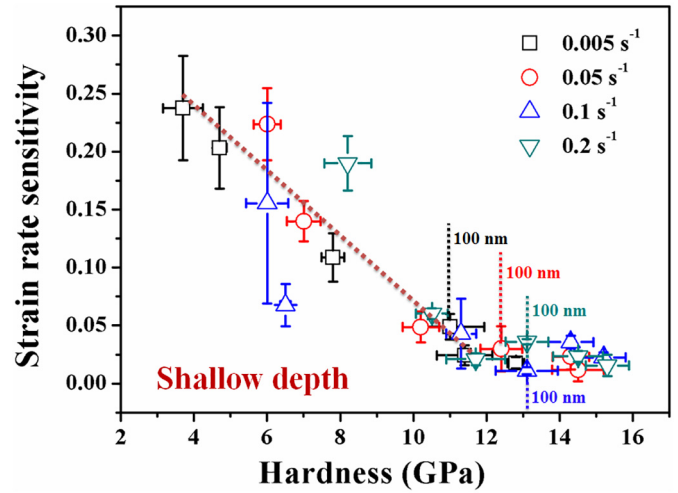$$V^* = b \times \xi \times l^* \qquad (13)$$

Fig. 7. The relationship between strain rate sensitivity (*m*) and hardness (*H*) [30] of BCC-Mo at settled LSRs (0.005–0.2 s^{-1}).

where *b* is the Burgers vector of the dislocations, ξ represents the height of a kink and it is a constant value (about one atomic distance) at a given temperature. l^* is termed as the critical distance between the two kinks in a kink-pair, which is the inverse proportional function of the square root of the applied stress [19,20]. According to Eq. (13), it had been indicated that the apparent activation volume of bcc metals was the function of the square of the applied stress as well, which should decrease to nearly constant under large applied stresses [19] such as the giga Pascal stresses underneath the indenter. As discussed in 4.2, the movement of screw-components in a mixed dislocation dominated the slip of a mixed dislocation at shallow penetration depths, therefore V^* was derived by the kink-pair nucleation of screw components and should be a constant value under the giga Pascal stress. Consequently, the value of *m* should be inversely proportional to hardness (*H*) according to Eq. (12). In addition, the relationship between *m* and *H* (inverse ISE) [30] was presented in Fig. 7. Apparently, the value of *m* decreased with increasing *H* at shallow penetration depth ($h < 100$ nm), which turned out the theoretical result.

4.4. LSR dependent m

The strength effect based on Eq. (12) could also explain the LSR dependent *m* at each penetration indentation depth. Faster LRS should result in higher hardness [3] and hence smaller *m*, which is consistent with the LSR dependent *m* observed in Fig. 4 and Fig. 7. In addition, as higher rate sensitivity was likely related to enhanced GB activities [47], the higher *m* derived at slower LSR indicated that more GB-mediated mechanisms might be involved. Since Coble creep and GBS were already ruled out as the dominant mechanism, interaction between dislocation and GBs was proposed as an alternative candidate, as elucidated below.

For NC metals, the stress required to nucleate a dislocation inside nanoscale grains (e.g., the present 38.4 nm grained Mo) was extremely high [48]. Therefore, dislocation sources located in grain interior could hardly operate, and dislocations might be emitted from and eventually absorbed by GBs [49]. The emission and absorption processes involving the interaction between dislocation and GBs were LSR dependent and could effectively alter the microstructural and local stress state in GB regions [27], as faster LSR causes higher local stress and more heterogeneous grain structures and vice versa. The generated high stress and heterogeneous structure at faster LSR during the loading period of indentation testing could effectively impede the emission and absorption of dislocations at GBs during the subsequent creep period. Accordingly, the strain rate sensitivity index at faster LSR was lower than that at

slower LSR, as interaction of dislocation and GB was a high rate-sensitive process in NC metals [50].

5. Conclusion

By evaluating the creep rate and strain rate sensitivity via nanoindentation creep testing, the indentation depth and LSR dependent creep deformation behavior of NC bcc-Mo thin films were systematically investigated. Specifically, the strain rate sensitivity *m* increased with decreasing indentation depth at each applied LSR, and faster LSR resulted in smaller *m* at given penetration depth. It was proposed that such variation trends of *m* were caused by the surface effect driven screw dislocation mobility as well as the unique dislocation structure within nano-sized grains. Even though the variation trends were somewhat similar to those derived from fcc metals or even metallic glasses, the present study demonstrated that the underlying creep mechanisms were tightly related to the bcc-characteristic-microstructures of NC Mo thin films, which might be quite different from those operating in other metallic atomic structures.

Acknowledgements

References

[1] K.D. Litasov, P.I. Dorogokupets, E. Ohtani, Y. Fei, A. Shatskiy, I.S. Sharygin, P.N. Gavryushkin, S.V. Rashchenko, Y.V. Seryotkin, Y. Higo, K. Funakoshi, A.D. Chanyshev, S.S. Lobanov, Thermal equation of state and thermodynamic properties of molybdenum at high pressures, J. Appl. Phys. 113 (2013) 093507.

[2] J.Y. Kim, D. Jang, J.R. Greer, Tensile and compressive behavior of tungsten, molybdenum, tantalum and niobium at the nanoscale, Acta Mater. 58 (2010) 2355–2363.

[3] W.D. Luo, D. Roundy, M.L. Cohen, J.W. Morris, Ideal strength of bcc molybdenum and niobium, Phys. Rev. B 66 (2002) 094110.

[4] J.W. Edwards, R. Speiser, H.L. Johnston, High temperature structure and thermal expansion of some metals as determined by x-ray diffraction data. I. Platinum, tantalum, niobium, and molybdenum, J. Appl. Phys. 22 (1951) 424.

[5] P. Schade, H.M. Ortner, I. Smid, Refractory metals revolutionizing the lighting technology: a historical review, Int. J. Refract. Met. Hard Mater. 50 (2015) 23–30.

[6] D.K. Song, X.Z. Xiao, J.M. Xue, H.J. Chu, H.L. Duan, Mechanical properties of irradiated multi-phase polycrystalline BCC materials, Acta Mech. Sinica 31 (2015) 191–204.

[7] K. Wang, D. Wang, F. Han, Effect of crystalline grain structures on the mechanical properties of twinning-induced plasticity steel, Acta Mech. Sinica 32 (2015) 181–187.

[8] D. Wu, J.Y. Zhang, J.C. Huang, H. Bei, T.G. Nieh, Grain-boundary strengthening in nanocrystalline chromium and the Hall–Petch coefficient of body-centered cubic metals, Scr. Mater. 68 (2013) 118–121.

[9] M.E. Kassner, M.-T. PeÂrez-Prado, Five-power-law creep in single phase metals and alloys, Prog. Mater. Sci. 45 (2000) 1–102.

[10] F.R.N. Nabarro, Creep in commercially pure metals, Acta Mater. 54 (2006) 263–295.

[11] G.S. Cho, G.B. Ahn, K.H. Choe, Creep microstructures and creep behaviors of pure molybdenum sheet at 0.7 T_m, Int. J. Refract. Met. Hard Mater. 60 (2016) 52–57.

[12] K.A. Darling, M. Rajagopalan, M. Komarasamy, M.A. Bhatia, B.C. Hornbuckle, R.S. Mishra, K.N. Solanki, Extreme creep resistance in a microstructurally stable nanocrystalline alloy, Nature 537 (2016) 378–381.

[13] Y.J. Wang, A. Ishii, S. Ogata, Entropic effect on creep in nanocrystalline metals, Acta Mater. 61 (2013) 3866–3871.

[14] C.L. Wang, Y.H. Lai, J.C. Huang, T.G. Nieh, Creep of nanocrystalline nickel: a direct comparison between uniaxial and nanoindentation creep, Scr. Mater. 62 (2010) 175–178.

[15] S. Vanpetegem, S. Brandstetter, B. Schmitt, H. Vanswygenhoven, Creep in nanocrystalline Ni during X-ray diffraction, Scr. Mater. 60 (2009) 297–300.

[16] T.G. Desai, P. Millett, D. Wolf, Is diffusion creep the cause for the inverse hall–Petch effect in nanocrystalline materials? Mater. Sci. Eng. A 493 (2008) 41–47.

[17] P.C. Millett, T. Desai, V. Yamakov, D. Wolf, Atomistic simulations of diffusional creep in a nanocrystalline body-centered cubic material, Acta Mater. 56 (2008) 3688–3698.

[18] Y. Ma, Y.H. Feng, T.T. Debela, G.J. Peng, T.H. Zhang, Nanoindentation study on the creep characteristics of high-entropy alloy films: fcc versus bcc structures, Int. J. Refract. Met. Hard Mater. 54 (2016) 395–400.

[19] Q. Wei, Strain rate effects in the ultrafine grain and nanocrystalline regimes—influence on some constitutive responses, J. Mater. Sci. 42 (2007) 1709–1727.

[20] Q. Wei, S. Cheng, K.T. Ramesh, E. Ma, Effect of nanocrystalline and ultrafine grain sizes on the strain rate sensitivity and activation volume: fcc versus bcc metals, Mater. Sci. Eng. A 381 (2004) 71–79.

[21] G.M. Cheng, W.W. Jian, W.Z. Xu, H. Yuan, P.C. Millett, Y.T. Zhu, Grain size effect on deformation mechanisms of nanocrystalline bcc metals, Math. Res. Lett. 1 (2013) 26–31.

[22] T.R. Malow, C.C. Koch, Mechanical properties, ductility, and grain size of nanocrystalline iron produced by mechanical attrition, Metall. Mater. Trans. A 29 (1998) 2285–2295.

[23] Q. Wei, Z.L. Pan, X.L. Wu, B.E. Schuster, L.J. Kecskes, R.Z. Valiev, Microstructure and mechanical properties at different length scales and strain rates of nanocrystalline tantalum produced by high-pressure torsion, Acta Mater. 59 (2011) 2423–2436.

[24] R.J. Klassen, B.J. Diak, S. Saimoto, Origin of the depth dependence of the apparent activation volume in polycrystalline 99.999% Cu determined by displacement rate change micro-indentation, Mater. Sci. Eng. A 387–389 (2004) 297–301.

[25] F. Wang, P. Huang, T.J. Lu, Surface-effect territory in small volume creep deformation, J. Mater. Res. 24 (2009) 3277–3285.

[26] A.A. Elmustafa, D.S. Stone, Nanoindentation and the indentation size effect-kinetics of deformation and strain gradient plasticity, J. Mech. Phys. Solids 51 (2003) 357–381.

[27] P. Huang, F. Wang, M. Xu, K.W. Xu, T.J. Lu, Dependence of strain rate sensitivity upon deformed microstructures in nanocrystalline Cu, Acta Mater. 58 (2010) 5196–5205.

[28] H. Li, A.H.W. Ngan, Size effects of nanoindentation creep, J. Mater. Res. 19 (2004) 513–522.

[29] F. Wang, P. Huang, K.W. Xu, Time dependent plasticity at real nanoscale deformation, Appl. Phys. Lett. 90 (2007) 161921.

[30] R. Saha, W.D. Nix, Effects of the substrate on the determination of thin film mechanical properties by nanoindentation, Acta Mater. 50 (2002) 23–38.

[31] J. Zhao, F. Wang, P. Huang, T.J. Lu, K.W. Xu, Depth dependent strain rate sensitivity and inverse indentation size effect of hardness in body-centered cubic nanocrystalline metals, Mater. Sci. Eng. A 615 (2014) 87–91.

[32] J.W. Mu, Z.H. Jiang, W.T. Zheng, H.W. Tian, J.S. Lian, Q. Jiang, High-speed creep process mediated by rapid dislocation absorption in nanocrystalline Cu, J. Appl. Phys. 111 (2012) 063506.

[33] Z.H. Cao, P.Y. Li, H.M. Lu, Y.L. Huang, Y.C. Zhou, X.K. Meng, Indentation size effects on the creep behavior of nanocrystalline tetragonal ta films, Scr. Mater. 60 (2009) 415–418.

[34] F. Wang, J.M. Li, P. Huang, W.L. Wang, T.J. Lu, K.W. Xu, Nanoscale creep deformation in Zr-based metallic glass, Intermetallics 38 (2013) 156–160.

[35] Y.J. Wang, A. Ishii, S. Ogata, Grain size dependence of creep in nanocrystalline copper by molecular dynamics, Mater. Trans. 53 (2012) 156–160.

[36] B.N. Lucas, W.C. Oliver, Indentation power-law creep of high-purity indium, Metall. Mater. Trans. A (1999) 601–610.

[37] Z.H. Cao, P.Y. Li, X.K. Meng, Nanoindentation creep behaviors of amorphous, tetragonal, and bcc Ta films, Mater. Sci. Eng. A 516 (2009) 253–258.

[38] Z.H. Cao, Q.W. She, Y.L. Huang, X.K. Meng, The rate sensitivity and plastic deformation of nanocrystalline tantalum films at nanoscale, Nanoscale Res. Lett. 6 (2011) 186.

[39] Z.H. Cao, H.M. Lu, X.K. Meng, A.H.W. Ngan, Indentation size dependent plastic deformation of nanocrystalline and ultrafine grain cu films at nanoscale, J. Appl. Phys. 105 (2009) 083521.

[40] H.J. Frost, M.F. Ashby, Deformation-Mechanism Maps: The Plasticity and Creep of Metals and Ceramics, 1st edition, Pergamon Press, 1982, pp. 1–166.

[41] Y.J. Wang, A. Ishii, S. Ogata, Transition of creep mechanism in nanocrystalline metals, Phys. Rev. B 84 (2011) 224102.

[42] R.L. Coble, A model for boundary diffusion controlled creep in polycrystalline materials, J. Appl. Phys. 34 (1963) 1679–1682.

[43] R. Raj, M.F. Ashby, On grain boundary sliding and diffusional creep, Metall. Mater. Trans. B 2 (1971) 1113–1127.

[44] D.M. Owen, T.G. Langdon, Low stress creep behavior: an examination of Nabarro—Herring and Harper—Dorn creep, Mater. Sci. Eng. A 216 (1996) 20–29.

[45] H. Luthy, R.A. White, O.D. Sherby, Grain-boundary sliding and deformation mechanism maps, Mater. Sci. Eng. 39 (1979) 211–216.

[46] D. Kaufmann, A.S. Schneider, R. Mönig, C.A. Volkert, O. Kraft, Effect of surface orientation on the plasticity of small bcc metals, Int. J. Plast. 49 (2013) 145–151.

[47] Y.J. Wei, A.F. Bower, H.J. Gao, Enhanced strain-rate sensitivity in fcc nanocrystals due to grain-boundary diffusion and sliding, Acta Mater. 56 (2008) 1741–1752.

[48] H. Van Swygenhoven, J.R. Weertman, Deformation in nanocrystalline metals, Mater. Today 9 (2006) 24–31.

[49] M. Dao, L. Lu, R. Asaro, J. Dehosson, E. Ma, Toward a quantitative understanding of mechanical behavior of nanocrystalline metals, Acta Mater. 55 (2007) 4041–4065.

[50] Y. Wang, A. Hamza, E. Ma, Temperature-dependent strain rate sensitivity and activation volume of nanocrystalline Ni, Acta Mater. 54 (2006) 2715–2726.